Lawrence Berkeley National Laboratory

Title
Understanding Origin of Voltage Hysteresis in Conversion Reaction for Na Rechargeable Batteries: The Case of Cobalt Oxides

Permalink
https://escholarship.org/uc/item/0fs0q391

Journal
Advanced Functional Materials, 26(28)

ISSN
1616-301X

Authors
Kim, Haegyeom
Kim, Hyunchul
Kim, Hyungsub
et al.

Publication Date
2016-07-01

DOI
10.1002/adfm.201601357

Peer reviewed

ADVANCED
FUNCTIONAL
MATERIALS
www.afm-journal.de

Materials
Views
www.MaterialsViews.com

FULL PAPER

Understanding Origin of Voltage Hysteresis in Conversion Reaction for Na Rechargeable Batteries: The Case of Cobalt Oxides

Haegyeom Kim, Hyunchul Kim, Hyungsub Kim, Jinsoo Kim, Gabin Yoon, Kyungmi Lim, Won-Sub Yoon, and Kisuk Kang*

Conversion reaction electrodes offer a high specific capacity in rechargeable batteries by utilizing wider valence states of transition metals than conventional intercalation-based electrodes and have thus been intensively studied in recent years as potential electrode materials for high-energy-density rechargeable batteries. However, several issues related to conversion reactions remain poorly understood, including the polarization or hysteresis during charge/discharge processes. Herein, Co_3O_4 in Na cells is taken as an example to understand the aforementioned properties. The large hysteresis in charge/discharge profiles is revealed to be due to different electrochemical reaction paths associated with respective charge and discharge processes, which is attributed to the mobility gap among inter-diffusing species in a metal oxide compound during de/sodiation. Furthermore, a Co_3O_4–graphene nanoplatelet hybrid material is demonstrated to be a promising anode for Na rechargeable batteries, delivering a capacity of 756 mAh g^{-1} with a good reversibility and an energy density of 96 Wh kg^{-1} (based on the total electrode weight) when combined with a recently reported $Na_4Fe_3(PO_4)_2(P_2O_7)$ cathode.

1. Introduction

Rechargeable battery chemistry has enabled modern mobile power and is disputably on the verge of application to large-scale energy storage systems integrated with renewable energy resources. Recently, Na rechargeable batteries have been widely studied as alternative energy storage devices that can compete with prevailing Li rechargeable batteries because of the widespread reserve of Na resources and potential cost merits suitable for such large-scale applications.[1–5] Na rechargeable batteries typically use cathodic (e.g., NaMnO$_2$, NaVPO$_4$F, NaFePO$_4$)[5–9] and anodic (e.g., graphite, hard carbon, NaTiO$_2$)[4,10–16] Na intercalation compounds, wherein Na ions are reversibly inserted and removed from the host structure. However, these compounds have exhibited a comparatively small capacity that intrinsically arises from the limited number of available Na interstitial sites in the crystalline host, resulting in a low energy density of the Na rechargeable batteries. To overcome this issue, recently, conversion reaction compounds, which have mostly been studied as high-capacity electrodes for Li rechargeable batteries,[17–25] have been investigated for possible high-capacity Na battery electrodes. Similar to the conversion reaction with Li, these compounds do not require Na sites in the crystalline host, and all possible valence states of transition metals (TMs) in the compound can be utilized, enabling more than one electron redox reaction per TM, which leads to a generally high specific capacity.[26–31]

In this respect, a few promising conversion reaction electrodes for Na storage have been identified, such as Co$_3$O$_4$ and Fe$_2$O$_3$, which exhibit reversible capacities of 400–500 mAh g^{-1}, while the search for additional new conversion reaction compounds remains active.[26,27,31–40] Despite recent intensive studies, many issues related to conversion reactions remain elusive, including the unusually large voltage polarization or hysteresis during cycles. The relatively large potential gap between charge and discharge processes is a common feature of conversion reaction compounds for Na rechargeable batteries and has also been universally observed for Li storage electrodes.[21,22,26,27,33,34,38] This large gap leads to an undesirably lower round-trip efficiency than the intercalation-based reactions. Although the origin of the large charge/discharge potential gap for conversion electrodes is not clearly understood, thus attracting tremendous interest,[41–44] a series of theoretical studies by the Ceder and Van der Ven groups proposes that the hysteresis in charge/discharge profiles is associated with different thermodynamic paths in charge and discharge

Dr. H. Kim,[+] Dr. H. Kim, Dr. J. Kim, G. Yoon, K. Lim,
Prof. K. Kang
Department of Materials Science and Engineering
Research Institute of Advanced Materials (RIAM)
Seoul National University
599 Gwanak-ro, Gwanak-gu, Seoul 151-742
Republic of Korea
E-mail: matlgen1@snu.ac.kr
H. Kim, Prof. W.-S. Yoon
Department of Energy Science
Sungkyunkwan University
Suwon 440-746, Republic of Korea
G. Yoon, Prof. K. Kang
Center for Nanoparticle Research
Institute for Basic Science (IBS)
Seoul National University
Seoul 151-742, Republic of Korea
[+]Present address: Lawrence Berkeley National Laboratory, 1 Cyclotron
Road, Berkeley, CA 94720, USA

www.MaterialsViews.com

ADVANCED
FUNCTIONAL
MATERIALS
www.afm-journal.de

FULL PAPER

processes.[42,45] First-principles multi-scale computations revealed that the (i) large mismatch in ionic mobilities between the Li (electrochemically active species) and displaced ionic species (mostly TMs) and (ii) insufficient thermodynamic driving force to redistribute displaced ions upon charging are attributed to different reaction paths in the conversion reactions.[45] Nevertheless, this idea has hardly been confirmed by experiments because of the difficulty in analyzing intermediate states during conversion and reconversion reactions resulting from the frequent formation of amorphous and nanosized products.

The present work carefully investigates Na conversion and reconversion reactions of Co_3O_4 using ex situ X-ray absorption spectroscopy (XAS), X-ray photoelectron spectroscopy (XPS), and transmission electron microscopy (TEM) analyses combined with electrochemical titration. It is experimentally verified that the hysteresis at pseudo open-circuit states results from two distinct reaction paths between conversion and reconversion, supporting the previous theoretical prediction. We further demonstrate that Co_3O_4 is a promising anode for Na rechargeable batteries when hybridized with graphene nanoplatelets, delivering a capacity of 756 mAh g^{-1} with good reversibility in a half cell. This hybrid material can deliver an energy

of 96 Wh kg^{-1} (based on the total electrode weight) when combined with an $Na_4Fe_3(PO_4)_2(P_2O_7)$ cathode in a full cell test.

2. Results and Discussion

2.1. Conversion and Reconversion Reactions of Co_3O_4 in Na Cells

The conversion reaction of the Co_3O_4 electrode was investigated in Na cells using commercial nanoparticles (Figure S1, Supporting Information). **Figure 1**a,b shows that the Co_3O_4 electrode was electrochemically active with Na delivering ≈500 mAh g^{-1} at ≈0.5 V (vs Na/Na$^+$). The discharge capacity and voltage profile are reminiscence of a typical Co_3O_4 conversion reaction in Li cells except for the lower voltage in the Na cell. The initial sodiation (discharge) voltage is noticeably lower than that in subsequent cycles in the cyclic voltammetry (CV) (Figure 1a) and galvanostatic measurements (Figure 1b). Even with the quasi-open-circuit potential (QOCP) measurements (Figure 1c), where the kinetically induced polarization is minimized, the first discharge and subsequent discharge reveal the
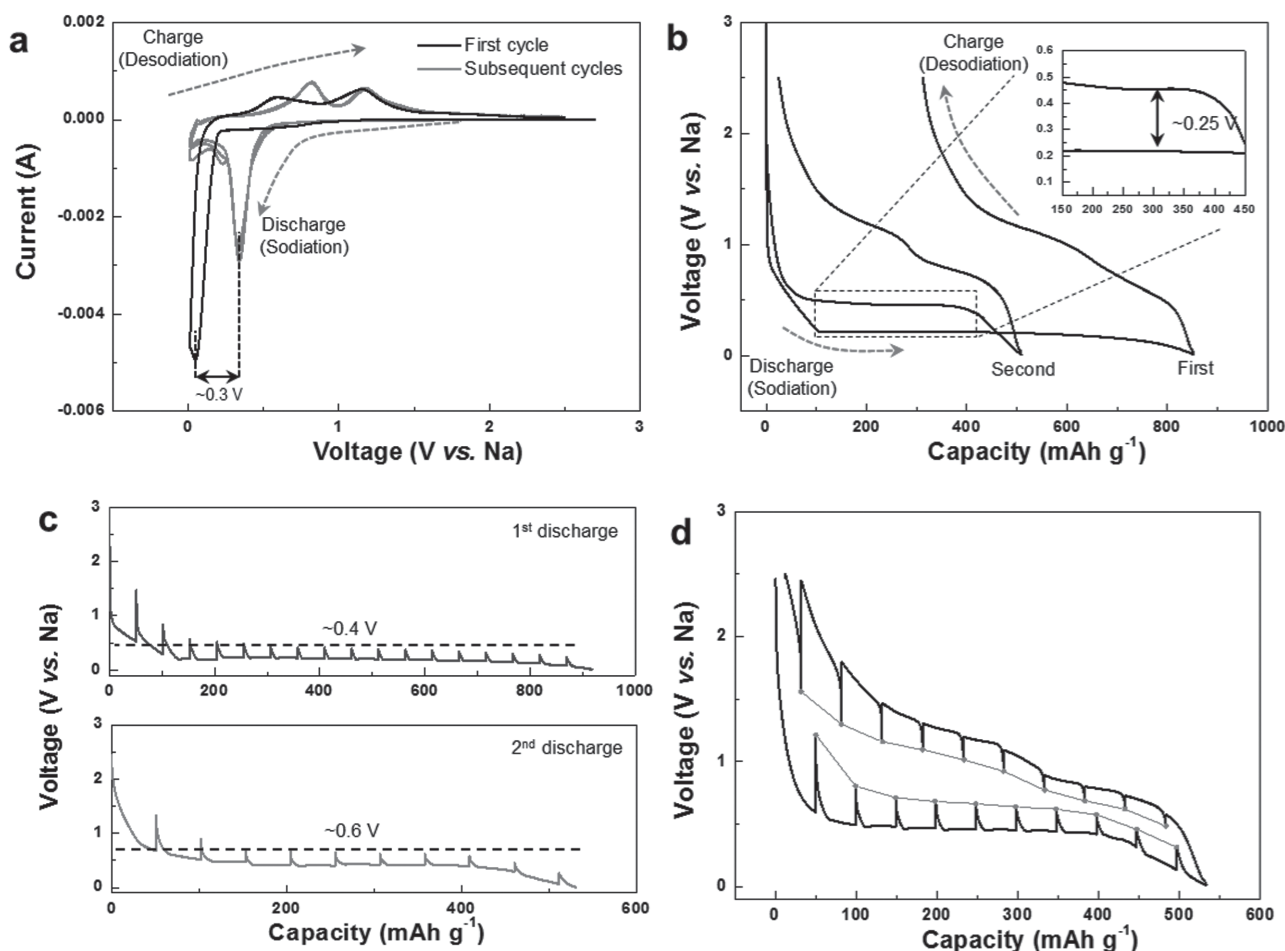

Figure 1. Electrochemical characterization of Co_3O_4 in Na rechargeable batteries. a) CV analysis and b) galvanostatic measurement of Co_3O_4 anode in Na half cells. c) QOCP analyses of Co_3O_4 anode in Na rechargeable batteries (above: first discharge, below: second discharge). d) QOCP analysis of Co_3O_4 anode during discharge and charge.
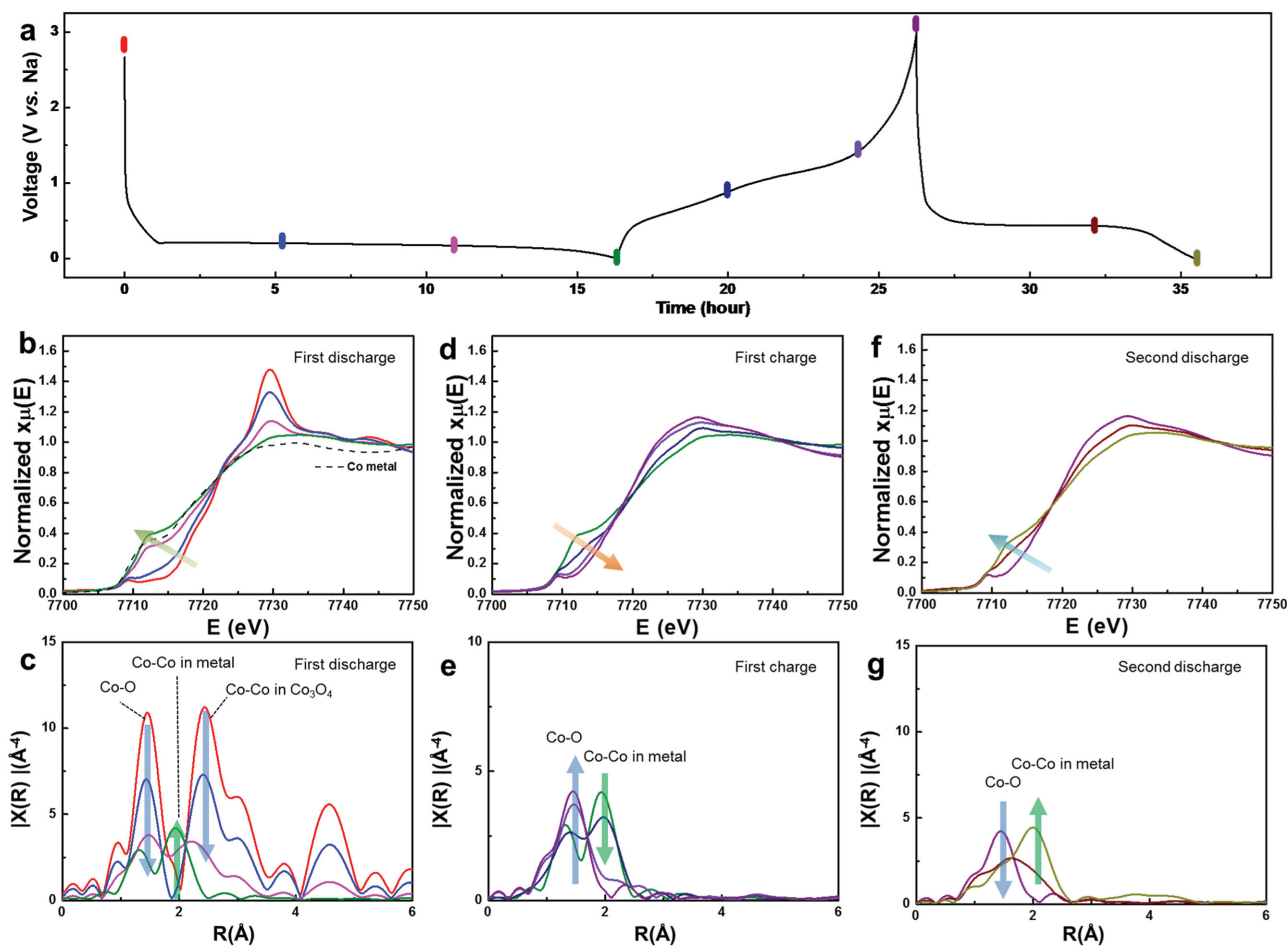
Figure 2. Ex situ XAS data coupled with electrochemical titration. a) Typical charge/discharge profiles at a current rate of 50 mA g⁻¹. b,d,f) Normalized Co K-edge XANES spectra and c,e,g) k^3-weighted Fourier transform magnitude of Co K-edge EXAFS spectra of Co_3O_4 anode. (– :pristine state, – : 33% state of first discharge, – : 66% state of first discharge, – : 100% state of first discharge, – : 33% state of first charge, – : 66% state of first charge, – :100% state of first charge, – : 60% state of second discharge, – : 100% state of second discharge).

apparently different voltage by ≈0.2 V. We used the 30 h relaxation time, where the rate of voltage change becomes less than ≈1 mV h⁻¹, indicating that further relaxation would not significantly change the potential (Figure S2, Supporting Information). This finding suggests that after the first cycle, the Co_3O_4 electrode has transformed to a state different from pristine Co_3O_4, which is most likely due to the formation of defective and/or nanosized Co_3O_4 particles during the cycle (Figure S3, Supporting Information).

Two oxidative peaks appear in the CV curve, whereas only a single reductive peak is observed throughout the cycles (Figure 1a). Similarly, the galvanostatic measurements and pseudo open-circuit potential in Figure 1b,d reveal that the charge profile exhibits non-single plateaus unlike the discharge profile with one distinct plateau. This result strongly suggests that the conversion and reconversion reactions would follow different reaction paths. To elucidate the discrepancy between the charge and discharge profiles, ex situ X-ray diffraction (XRD) analysis was conducted in Na cells at different states of discharge and charge; however, the XRD patterns revealed an amorphous-like nature after the sodiation, which was not recovered after the desodiation. This type of behavior is generally

observed in the conversion reactions because of the small particulate size of the discharge products (Figure S4, Supporting Information).[31,46] To obtain insight into the structural evolution of the Co_3O_4 electrode, ex situ XAS analyses coupled with electrochemical titration were further performed. **Figure 2** presents the detailed conversion and reconversion reactions of the Co_3O_4 electrode in Na cells. During the first discharge, the decrease in the average oxidation of Co is clearly observable; the Co K-edge X-ray absorption near-edge structure (XANES) spectra in Figure 2b shift toward lower energy values, and the valence state of Co nearly approaches that of Co metal at the end of discharge. In the extended X-ray absorption fine structure (EXAFS) spectra for this process in Figure 2c, the reduction of Co ions is accompanied by a change in the local environment around the Co atom. The first peak at ≈1.4 Å in the Co K-edge spectra corresponds to the Co—O bonds, and the broad peaks in the region of 2.0–4.0 Å originate from the Co—Co interactions in the crystalline Co_3O_4. Upon discharge, the peak intensities of Co—O and Co—Co notably decrease, and a new Co—Co peak corresponding to the Co metal appears at ≈1.9 Å, which clearly confirms the conversion reaction of Co_3O_4 with Na. During the charge process, the Co K-edge XANES spectra shift

www.MaterialsViews.com

ADVANCED
FUNCTIONAL
MATERIALS
www.afm-journal.de

FULL PAPER

back toward higher energy values (Figure 2d), and the EXAFS spectra reveal the rise of nearest Co—O bonding and decrease of Co—Co peaks from Co metal, implying that the reconversion reaction occurs (Figure 2e). However, the valence state of Co and long-range ordering peaks ($>\approx 3$ Å) are not completely recovered to the pristine state, which is attributed to the formation of defective $Co_3O_{4-\delta}$ or fine particles and agrees well with the XRD analysis. During the second discharge, the reduction of Co ions and recovery of Co—Co bonding occur at the expense of Co—O bonding (Figure 2f,g), following the reverse process of the first charge shown in Figure 2d,e. However, the EXAFS profile change in the second discharge differs significantly from that during the first discharge in Figure 2c: No noticeable EXAFS peaks are observed at $>\approx 3$ Å in the second discharge process. This result implies that the pristine long-range ordering is permanently lost during the subsequent cycles. We expect this phenomenon is responsible for the different charge/discharge profiles between the first and subsequent cycles, while side reactions including irreversible electrolyte decomposition and its reaction with the electrode surface to form a solid electrolyte interphase will contribute to it to some extent.

2.2. Probing Conversion and Reconversion Paths

We further employed ex situ XPS and TEM analyses to probe the local environment of Co in the reactants and products during electrochemical reaction. The ex situ XPS analysis in **Figure 3**b and Figure S5 (Supporting Information) reveals that a XPS peak corresponding to Co metal gradually appears at the expense of the $Co^{+8/3}$ peak upon discharge, confirming the phase transformation involving Co_3O_4 and metallic Co, which is consistent with the XAS results.[47–49] Interestingly, however, the reverse behavior is not observed during the reconversion; instead, a new peak (≈ 778 eV) appears at the 50% state of charge (SOC), which does not correspond to either $Co^{+8/3}$ or Co^0. Further charge changes the valence state of Co back to that of Co_3O_4, which indicates that the reconversion is not a simple step involving only Co_3O_4 and metallic Co but passes through an intermediate state that was not experienced during conversion. To quantify the valence state of the observed Co peak (≈ 778 eV) in the 50% SOC, the relation between the XPS binding energy and valence states of Co for several known compounds (CoO_2, $Co(OH)_2$, $LiCoO_2$, CoO,
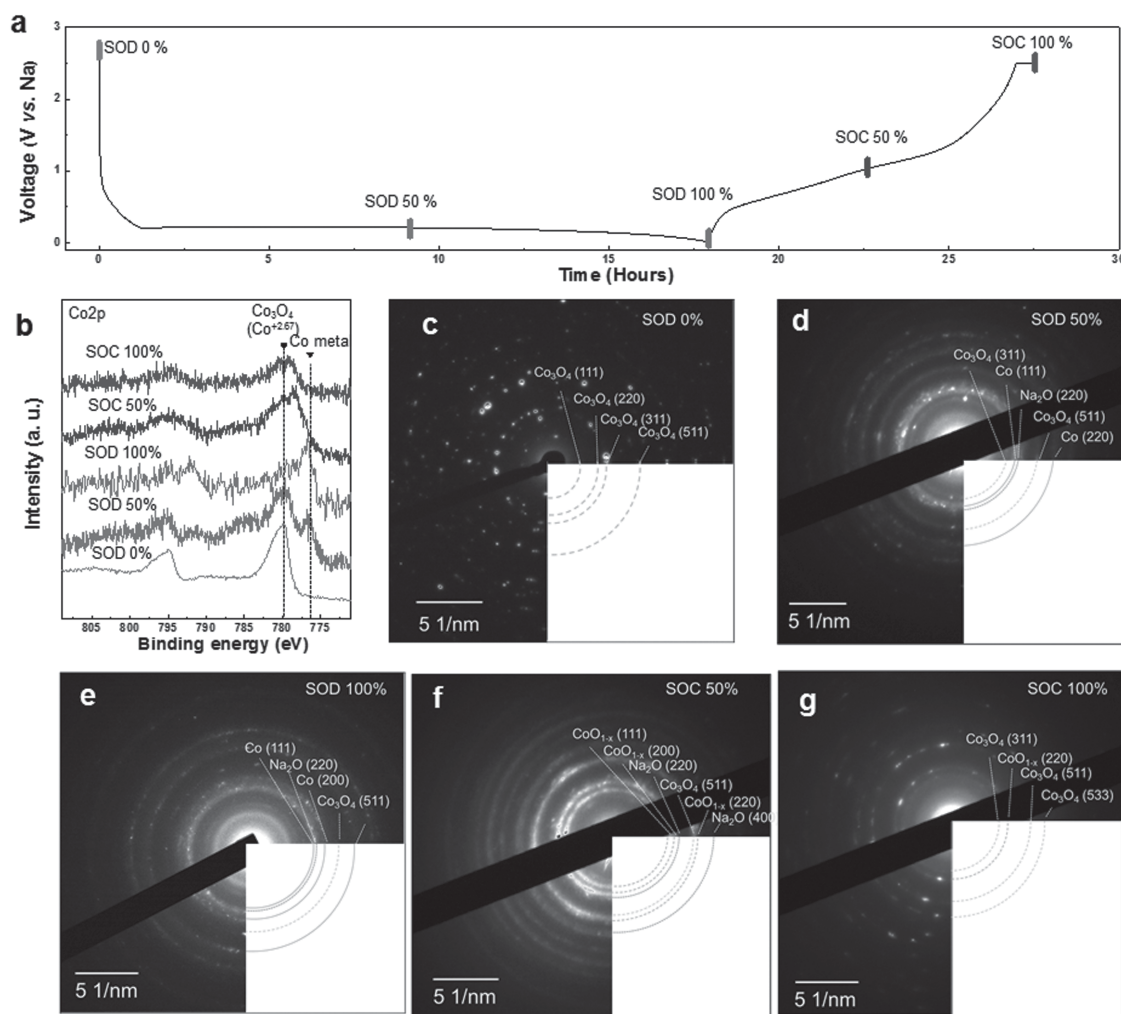

Figure 3. Ex situ TEM and XPS analyses of Co_3O_4 anode after de/sodiation for the first cycle. a) Typical charge/discharge profile at a current rate of 50 mA g^{-1}. b) XPS measurements at each state of discharge and charge. c–g) Selected area electron diffraction data of the Co_3O_4 after de/sodiation.

ADVANCED
FUNCTIONAL
MATERIALS
www.afm-journal.de

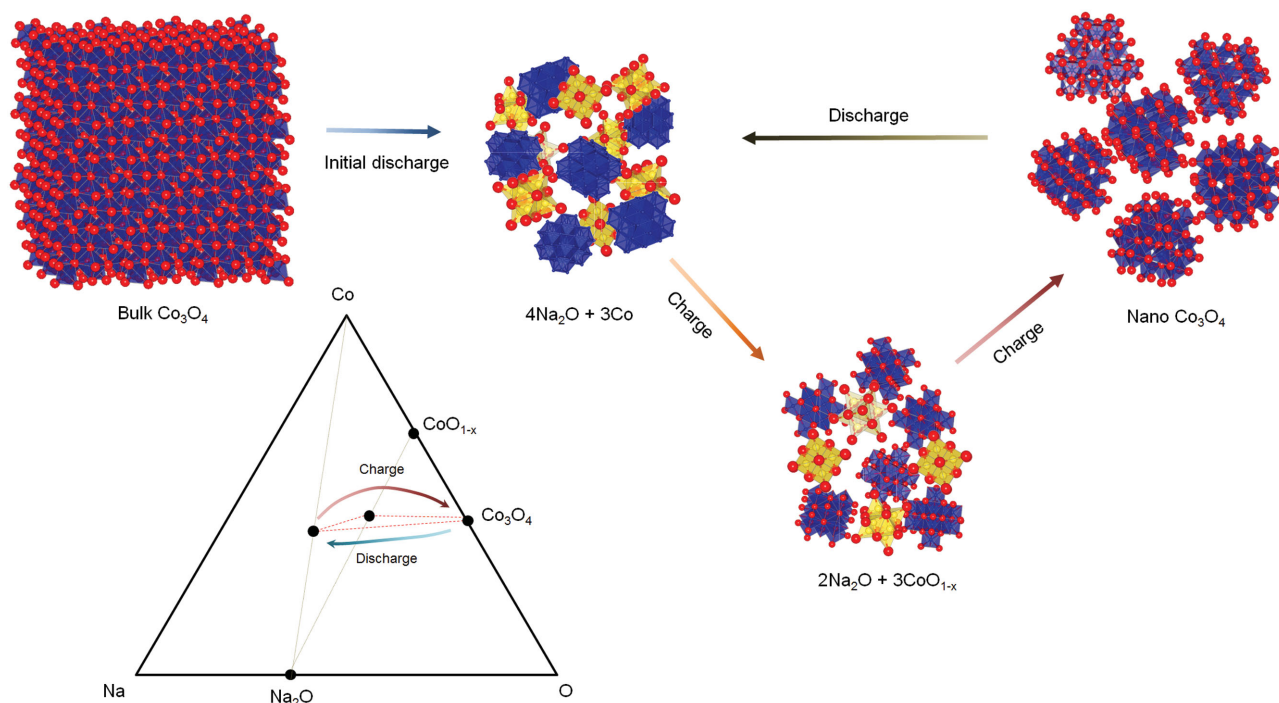Materials
Views
www.MaterialsViews.com

Figure 4. Schematics of conversion and reconversion reaction mechanism for Co_3O_4 in Na rechargeable batteries.

Co) is plotted in Figure S6 (Supporting Information). This plot reveals that the valence state of the observed Co peak ($\approx$778 eV) is estimated to be +1.15, indicating the formation of an intermediate compound of CoO_{1-x} ($x = \approx$0.425).[48–52] The ex situ TEM analysis in Figure 3c–g supports the formation of this intermediate CoO_{1-x} phase during the reconversion. Although the conversion reaction of Co_3O_4 to metallic Co and Na_2O is confirmed in Figure 3c–e, a CoO-like phase (CoO_{1-x}) is clearly observed in the 50% SOC sample in Figure 3f and Figure S7 (Supporting Information), which is consistent with the XPS analysis. Based on our TEM and XPS observations, we expect that the intermediate phase obtained at 50% SOC is most likely the oxygen deficient CoO_{1-x}, while further study is required to determine the precise crystal structure of the intermediate phase (CoO_{1-x}). After further charge, the Co_3O_4 phase finally appears at the expense of Na_2O and CoO_{1-x} (Figure 3g). Note that the two-step charging process involving an intermediate state is consistent with the CV and galvanostatic measurements in Figure 1, which reveal two oxidative peaks and a non-single plateau during the charging unlike the discharge process. The morphology and distribution of metallic Co in the discharged state were also carefully examined using HRTEM (Figure S8, Supporting Information). When sodiation occurs in Co_3O_4, Co metal and Na_2O nanodomains are observed as a mixture, which agrees with our ex situ XRD characterization and XAS analysis. Note that Na_2O was formed instead of NaO_2 or Na_2O_2 in contrast to the results for Na–O_2 batteries.[53,54]

Based on these observations, the Na storage mechanism in Co_3O_4 is proposed and summarized in **Figure 4**. During the initial discharge, the sodiation of bulk Co_3O_4 leads to the formation of a nanocomposite of Na_2O and Co without

the appearance of an intermediate phase. However, during the subsequent charging process, a CoO_{1-x} intermediate phase evolves at the expense of Na_2O and Co metal at the early stage. Further charging induces the transformation of the composite of Na_2O and CoO_{1-x} into nano Co_3O_4. Subsequent discharge forms a nanocomposite of Na_2O and Co metal from the nano Co_3O_4. The observed distinct paths in the conversion and reconversion reactions can be understood in the context of an inter-diffusion problem in a ternary system. A phase evolution process at low temperature often follows the reaction path that can be kinetically reached rather than the most thermodynamically stable path.[42,55] In ternary systems, the intermediate compositions do not have to follow a linear path between the compositions of two inter-diffusing phases. Rather, the intermediate compositions can follow a curved, kinetically favorable path in the phase diagram according to the relative diffusivity of each species, as indicated in Figure 4.[55] This result occurs because the faster-moving species favor the formation of a selective equilibrium state, whereas the slower-moving species follow a non-equilibrium distribution. In this scenario, the Co cation, which is more mobile than the O anion, would like to form a Co-rich phase such as CoO_{1-x} (in other words, an O-deficient phase) at the interface between Na_2O and Co when Na ions are extracted from the discharged products because cations move faster than anions. However, when Na ions are inserted into Co_3O_4, Co will be easily segregated from the oxygen-forming metallic Co because of the more mobile Na ions that take up oxygen.[56,57] Based on this principle, the diffusivity gap among three inter-diffusing species (Na, Co, and O) is considered a driving force for the hysteresis in the conversion reactions.

2.3. Co₃O₄–Graphene Hybrid Anode for Na Rechargeable Batteries

Having verified the feasibility of conversion-based Na storage, the practical validity of Co₃O₄ in Na rechargeable batteries was further examined using a hybrid material of Co₃O₄-decorated graphene nanoplatelets. The XRD pattern of the hybrid material in **Figure 5**a is consistent with cubic spinel Co₃O₄ (space group: *Fd-3m*) without impurities. Raman analysis confirmed the phases of Co₃O₄ and graphene, as shown in Figure 5b.[19] The morphology and distribution of Co₃O₄ on graphene nanoplatelets were examined using field-emission scanning electron microscopy (FESEM) and TEM analyses (Figure 3c–d and Figures S9–S11, Supporting Information), which revealed wrinkled graphene decorated with Co₃O₄ (≈5 nm) based on energy dispersive spectroscopy (EDS) analysis (Figure S9, Supporting Information). The EDS mapping and line scanning reveal that the Co₃O₄ particles are uniformly distributed on the graphene nanoplatelets without segregation (Figures S9 and S10, Supporting Information). The content of graphene nanoplatelets in the hybrid materials was measured to be 18.3 wt% using an elemental analyzer.

The charge/discharge profiles of the Co₃O₄–graphene hybrid material at a current rate of 100 mA g⁻¹ are presented in Figure 5e. The hybrid material delivered a capacity of 1203 mAh g⁻¹ in the first discharge and a reversible capacity of 756 mAh g⁻¹ (≈85% of the theoretical capacity) when the capacity was calculated with the weight of Co₃O₄ in the electrode. Note that the graphene nanoplatelets deliver ≈200 mAh g⁻¹ when cycled alone in the voltage range of 2.5–0.01 V with a slopy profile (Figure S12, Supporting Information). Considering the graphene content in the hybrid material (18.3 wt%), the contribution of the graphene nanoplatelets to the capacity of the hybrid material is only ≈37 mAh g⁻¹. When the specific capacity was calculated using the total weight of hybrid material including Co₃O₄ and graphene, the reversible capacity was 617.6 mAh g⁻¹. The irreversible capacity obtained at the first discharge could be associated with the formation of a solid–electrolyte interphase on the electrode surface.[20] After the first discharge, the charge/discharge profiles are not significantly altered (Figure 5e), which indicates that the hybrid material is tolerant of the reversible sodiation and desodiation even though the capacity gradually decreased upon cycling. Furthermore, the hybrid material maintains ≈451 mAh g⁻¹ after 50 cycles with a relatively high coulombic efficiency (≈98%), which is comparable to or even better than recently reported values.[26,33,58,59] However, the bare Co₃O₄ nanoparticles exhibit a rapid capacity fading (Figure 5f). When the content of conductive carbon in the electrode increases, the cycle stability is slightly improved; however, the improvement in cycle stability remains far below that of the Co₃O₄–graphene nanoplatelet hybrid material. The hybrid materials maintain their nanostructure, in which Co₃O₄ nanoparticles are well distributed on the graphene nanoplatelets without segregation even after repeated battery operation (Figures S13 and S14, Supporting Information).[19] Nevertheless, the cycle stability of Co₃O₄-graphene hybrid anode is still insufficient for practical applications and thus further improvement is required.

The electrochemical performance of the Co₃O₄–graphene hybrid material was further examined in a full cell with an Na₄Fe₃(PO₄)₂(P₂O₇) cathode, which has recently been reported as a potential cathode for Na-ion batteries.[60] Figure S15 (Supporting Information) presents the charge/discharge profile of Na₄Fe₃(PO₄)₂(P₂O₇) at a current rate of 50 mA g⁻¹, which delivers a reversible capacity of 90 mAh g⁻¹ with an average voltage of 3.2 V versus Na. A typical charge/discharge profile of full cells is presented in Figure 5g. Full cells were constructed using a Co₃O₄–graphene hybrid anode and Na₄Fe₃(PO₄)₂(P₂O₇) cathode with a 1:6 ratio for weight. The full cell delivers a reversible capacity of ≈470 mAh g⁻¹ based on the anode active materials. In this configuration, an energy density of ≈96 Wh kg⁻¹ was obtained (based on the total mass of both electrodes), while the energy efficiency was ≈50% due to the large voltage hysteresis of Co₃O₄–graphene anode. Although further improvement of both the half cell efficiency and full cell performance are necessary for such a nascent chemistry to become practical, Co₃O₄–graphene hybrid materials are prospective anodes for high-performance Na-ion batteries.

3. Conclusion

Herein, the Na conversion and reconversion reactions in a Co₃O₄ anode were carefully investigated using electrochemical measurements, XAS, XPS, and HRTEM coupled with electrochemical titration. It was experimentally verified for the first time that the large hysteresis in charge/discharge profiles results from the different thermodynamic paths of conversion and reconversion reactions. The formation of an intermediate phase (CoO₁₋ₓ) only occurring during the charge process is the root cause of the hysteresis and was attributed to the mobility gap among three inter-diffusing species (Na, Co, and O) in a metal oxide compound. The Co₃O₄–graphene nanoplatelet hybrid material delivered a capacity of 756 mAh g⁻¹ with good reversibility in a half cell and an energy of 96 Wh kg⁻¹ (based on the total electrode weight) combined with an Na₄Fe₃(PO₄)₂(P₂O₇) cathode in a full cell, indicating its potential applicability as a high-capacity anode for Na rechargeable batteries.

4. Experimental Section

Fabrication of Co₃O₄–Graphene Nanoplatelet Hybrid Materials: Co₃O₄–graphene nanoplatelet hybrid materials were synthesized following the previously reported method.[19] Graphite oxide was prepared from natural graphite powder, wherein graphite (Bay Carbon, 1 g), NaNO₃ (Aldrich, 1 g), and H₂SO₄ (Aldrich, 45 mL) were stirred in an ice bath for 30 min followed by the addition of KMnO₄ (Aldrich, 5 g). The mixture was stirred for 2 h at 40 °C followed by the addition of deionized (DI) water (100 mL). The resultant solution was filtered and washed with 150 mL of HCl (10%) and 100 mL of DI water. The graphite oxide (100 mg) was dispersed in DI water (400 mL), and the solution was sonicated for 90 min to produce graphene oxide. Cobalt acetate tetrahydrate ((C₂H₃O₂)₂Co·4H₂O), Aldrich, 350 mg) and DI water (400 mL) were added to the graphene oxide solution. Then, 4.0 mL of NH₄OH (Aldrich) and 0.3 mL of hydrazine (NH₂NH₂, 35 wt%, Aldrich) were added, followed by stirring for 4 h at 100 °C. The resultant solution was filtered and washed with DI water. Finally, the filtered powder was heated at 200 °C for 6 h in air.
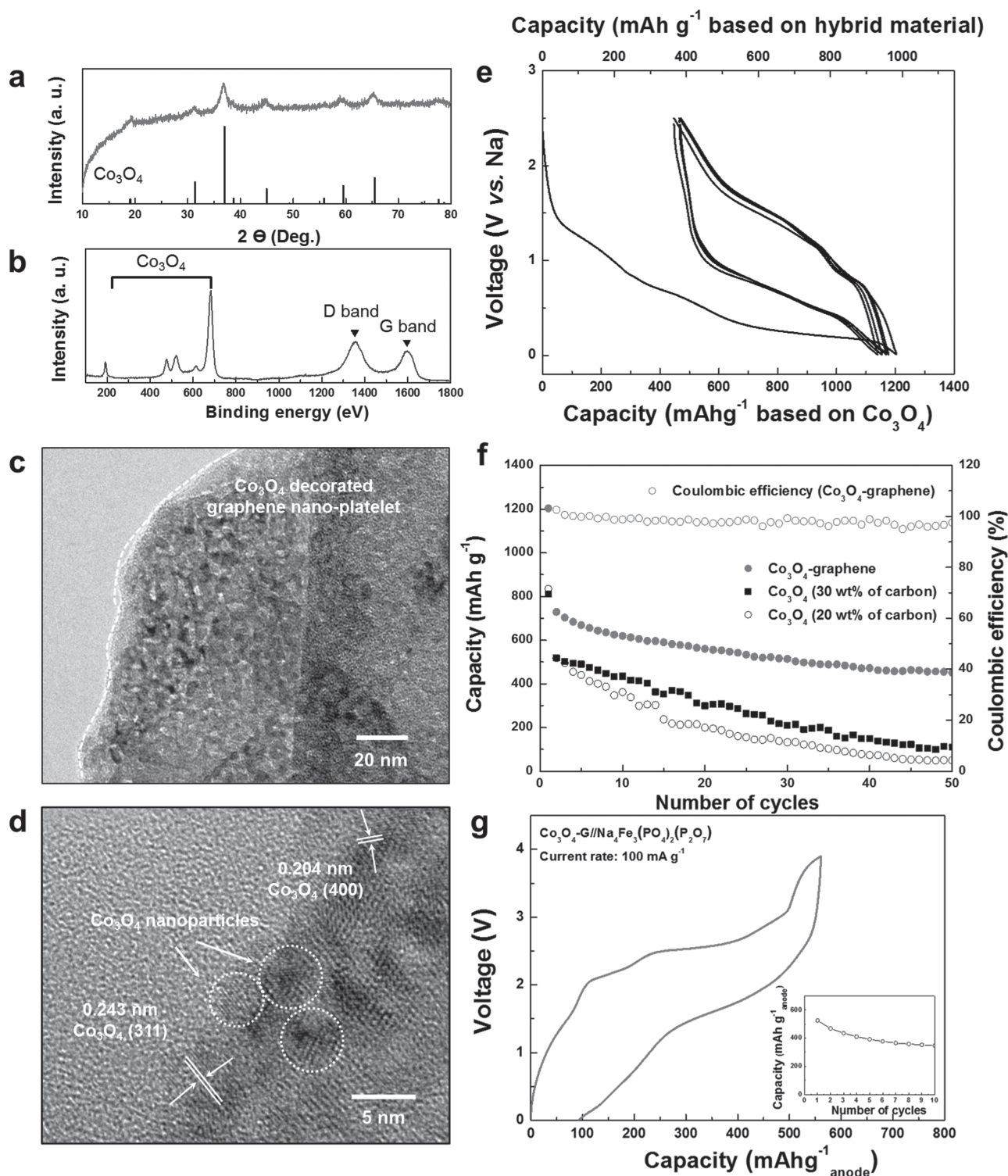
ADVANCED
FUNCTIONAL
MATERIALS
www.afm-journal.de

Materials
Views
www.MaterialsViews.com

Figure 5. Characterization of Co_3O_4–graphene hybrid material and its electrochemical performance in Na rechargeable batteries. a) XRD pattern, b) Raman analysis, and c,d) TEM images of Co_3O_4–graphene hybrid materials. These results confirm that Co_3O_4 nanoparticles are uniformly distributed on graphene nanoplatelets. e) Charge/discharge profiles and f) cycle stability of Co_3O_4–graphene hybrid materials compared with Co_3O_4 nanoparticles. g) A typical charge/discharge profile of full cells consisting of a Co_3O_4–graphene hybrid anode and $Na_4Fe_3(PO_4)_2(P_2O_7)$ cathode (inset: cyclability).

www.MaterialsViews.com

ADVANCED
FUNCTIONAL
MATERIALS
www.afm-journal.de

FULL PAPER

Characterization: The crystal structure of the samples was analyzed with an X-ray diffractometer (D2PHASER) using Cu Kα radiation. XPS (PHI 5000 VeraProbe) was used to determine the valence states of the sample. For the ex situ XPS measurements, all the steps for the sample preparation were conducted in an Ar-filled glove box to prevent any contamination. The morphology of the samples was verified using FESEM (SUPRA 55VP) and HRTEM (Tecnai F20).

For the ex situ XAS experiments, electrode samples were prepared at different states of charge by disassembling the coin cells in an Ar-filled glovebox. The collected electrodes were washed using anhydrous diethyl carbonate. XAS spectra were collected at the facility installed at beamline 7D at PLS-II located at Pohang Accelerator Laboratory in transmission mode with N_2 gas ionization detectors and an Si(111) double crystal monochromator detuned to ≈70% of its original intensity to eliminate higher-order harmonics. The storage ring was operated at 2.5 GeV with a ring current of 100–150 mA. Reference spectra of the Co metal were collected simultaneously using Co foil. The XAS data were analyzed using the Athena program.[61] The extracted EXAFS signal, $\chi(k)$, was weighted by k^3 to emphasize the high-energy oscillations and then Fourier-transformed in a k range from 2.0 to 10.8 Å^{-1} for the Co K-edge using a Hanning window to obtain magnitude plots of the EXAFS spectra in R-space (Å). The Co_3O_4–graphene hybrid material was analyzed using a high-resolution dispersive Raman microscope (LabRAM HR UV–vis–NIR) with Raman shifts from 100 to 1800 cm^{-1}.

Electrodes were prepared by mixing the active material (Co_3O_4 nanoparticles, 70 wt%) with polyvinylidene fluoride binder (PVDF, 10 wt%) and conductive carbon black (20 wt%) in an N-methyl-2-pyrrolidone (NMP) solvent. The resulting slurry was uniformly pasted onto Al foil, dried at 120 °C for 2 h, and roll-pressed. The electrode thickness and loading density of Co_3O_4 nanoparticles were ≈35 μm and 1.8 mg cm^{-2}, respectively. Test cells were assembled in a glove box into a two-electrode configuration with an Na metal counter electrode. A grade GF/F separator (Whatman, USA) was used, and 1 M NaPF$_6$ in diethylene glycol dimethyl ether (DEGDME) was used as the electrolyte. Electrochemical profiles were obtained over a voltage range from 2.5 to 0.01 V using a multichannel potentio-galvanostat (WonATech). QOCPs were measured using a constant current of 50 mA g^{-1} followed by a 30 h relaxation time.

The Co_3O_4–graphene nanoplatelet hybrid material electrodes were prepared by mixing the hybrid material (80 wt%), PVDF (10 wt%), and conductive carbon black (10 wt%) in NMP solvent. The slurry was pasted onto Al foil, dried at 120 °C for 2 h, and roll-pressed. The electrode thickness and loading density of the hybrid material were ≈33 μm and 1.6 mg cm^{-2}, respectively. $Na_4Fe_3(PO_4)_2(P_2O_7)$ electrodes were similarly fabricated by mixing with PVDF binder and conductive carbon black at a weight ratio of 70:20:10 in NMP solvent. The $Na_4Fe_3(PO_4)_2(P_2O_7)$ electrodes were cycled in the voltage range of 2.5–4.3 V at a current rate of 50 mA g^{-1}. A full cell was assembled using a Co_3O_4–graphene nanoplatelet anode and $Na_4Fe_3(PO_4)_2(P_2O_7)$ cathode with a 1:6 ratio for weight, in which 1 M NaPF$_6$ in DEGDME electrolyte was used. Before assembling the full cell, the Co_3O_4–graphene anode was pre-cycled in a half cell configuration. The full cell was cycled in the voltage window between 0.01 and 3.9 V at a current rate of 100 mA g^{-1}.

Supporting Information

Supporting Information is available from the Wiley Online Library or from the author.

Acknowledgements

[1] M. D. Slater, D. Kim, E. Lee, C. S. Johnson, *Adv. Funct. Mater.* **2013**, *23*, 947.

[2] S.-W. Kim, D.-H. Seo, X. Ma, G. Ceder, K. Kang, *Adv. Energy Mater.* **2012**, *2*, 710.

[3] V. Palomares, P. Serras, I. Villaluenga, K. B. Hueso, J. Carretero-Gonzalez, T. Rojo, *Energy Environ. Sci.* **2012**, *5*, 5884.

[4] H. Kim, J. Hong, Y.-U. Park, J. Kim, I. Hwang, K. Kang, *Adv. Funct. Mater.* **2015**, *25*, 534.

[5] X. Xiang, K. Zhang, J. Chen, *Adv. Mater.* **2015**, *27*, 5343.

[6] J. Zhao, J. He, X. Ding, J. Zhou, Y. o. Ma, S. Wu, R. Huang, *J. Power Sources* **2010**, *195*, 6854.

[7] X. Ma, H. Chen, G. Ceder, *J. Electrochem. Soc.* **2011**, *158*, A1307.

[8] Y. Lu, S. Zhang, Y. Li, L. Xue, G. Xu, X. Zhang, *J. Power Sources* **2014**, *247*, 770.

[9] S.-M. Oh, S.-T. Myung, J. Hassoun, B. Scrosati, Y.-K. Sun, *Electrochem. Commun.* **2012**, *22*, 149.

[10] H. Kim, J. Hong, G. Yoon, H. Kim, K.-Y. Park, M.-S. Park, W.-S. Yoon, K. Kang, *Energy Environ. Sci.* **2015**, *8*, 2963.

[11] B. Jache, P. Adelhelm, *Angew. Chem., Int. Ed.* **2014**, *53*, 10169.

[12] Z. Zhu, F. Cheng, Z. Hu, Z. Niu, J. Chen, *J. Power Sources* **2015**, *293*, 626.

[13] S. Komaba, W. Murata, T. Ishikawa, N. Yabuuchi, T. Ozeki, T. Nakayama, A. Ogata, K. Gotoh, K. Fujiwara, *Adv. Funct. Mater.* **2011**, *21*, 3859.

[14] A. Ponrouch, A. R. Goñi, M. R. Palacín, *Electrochem. Commun.* **2013**, *27*, 85.

[15] Y. Cao, L. Xiao, M. L. Sushko, W. Wang, B. Schwenzer, J. Xiao, Z. Nie, L. V. Saraf, Z. Yang, J. Liu, *Nano Lett.* **2012**, *12*, 3783.

[16] D. Wu, X. Li, B. Xu, N. Twu, L. Liu, G. Ceder, *Energy Environ. Sci.* **2015**, *8*, 195.

[17] Y. Li, B. Tan, Y. Wu, *Nano Lett.* **2008**, *8*, 265.

[18] H. Wang, L.-F. Cui, Y. Yang, H. S. Casalongue, J. T. Robinson, Y. Liang, Y. Cui, H. Dai, *J. Am. Chem. Soc.* **2010**, *132*, 13978.

[19] H. Kim, D.-H. Seo, S.-W. Kim, J. Kim, K. Kang, *Carbon* **2011**, *49*, 326.

[20] Z.-S. Wu, W. Ren, L. Wen, L. Gao, J. Zhao, Z. Chen, G. Zhou, F. Li, H.-M. Cheng, *ACS Nano* **2010**, *4*, 3187.

[21] P. L. Taberna, S. Mitra, P. Poizot, P. Simon, J. M. Tarascon, *Nat. Mater.* **2006**, *5*, 567.

[22] H. Kim, S.-W. Kim, J. Hong, Y.-U. Park, K. Kang, *J. Mater. Res.* **2011**, *26*, 2665.

[23] P. Poizot, S. Laruelle, S. Grugeon, L. Dupont, J. M. Tarascon, *Nature* **2000**, *407*, 496.

[24] X. Zhu, Y. Zhu, S. Murali, M. D. Stoller, R. S. Ruoff, *ACS Nano* **2011**, *5*, 3333.

[25] G. Zhou, D.-W. Wang, F. Li, L. Zhang, N. Li, Z.-S. Wu, L. Wen, G. Q. Lu, H.-M. Cheng, *Chem. Mater.* **2010**, *22*, 5306.

[26] M. M. Rahman, A. M. Glushenkov, T. Ramireddy, Y. Chen, *Chem. Commun.* **2014**, *50*, 5057.

[27] Z. Jian, P. Liu, F. Li, M. Chen, H. Zhou, *J. Mater. Chem. A* **2014**, *2*, 13805.

[28] M. M. Rahman, I. Sultana, Z. Chen, M. Srikanth, L. H. Li, X. J. Dai, Y. Chen, *Nanoscale* **2015**, *7*, 13088.

[29] F. Klein, B. Jache, A. Bhide, P. Adelhelm, *Phys. Chem. Phys. Chem.* **2013**, *15*, 15876.

[30] S.-M. Oh, S.-T. Myung, C. S. Yoon, J. Lu, J. Hassoun, B. Scrosati, K. Amine, Y.-K. Sun, *Nano Lett.* **2014**, *14*, 1620.

[31] D. Y. W. Yu, P. V. Prikhodchenko, C. W. Mason, S. K. Batabyal, J. Gun, S. Sladkevich, A. G. Medvedev, O. Lev, *Nat. Commun.* **2013**, *4*, 2922.

FULL PAPER

[32] J. Yang, T. Zhou, R. Zhu, X. Chen, Z. Guo, J. Fan, H. K. Liu, W.-X. Zhang, *Adv. Mater. Interfaces* **2016**, *3*, 1500464.

[33] J.-W. Wen, D.-W. Zhang, Y. Zang, X. Sun, B. Cheng, C.-X. Ding, Y. Yu, C.-H. Chen, *Electrochim. Acta* **2014**, *132*, 193.

[34] Z. Jian, B. Zhao, P. Liu, F. Li, M. Zheng, M. Chen, Y. Shi, H. Zhou, *Chem. Commun.* **2014**, *50*, 1215.

[35] S. Wang, W. Wang, P. Zhan, S. Jiao, *ChemElectroChem* **2014**, *1*, 1636.

[36] K. Zhang, Z. Hu, X. Liu, Z. Tao, J. Chen, *Adv. Mater.* **2015**, *27*, 3305.

[37] S. Yuan, X.-L. Huang, D.-L. Ma, H.-G. Wang, F.-Z. Meng, X.-B. Zhang, *Adv. Mater.* **2014**, *26*, 2273.

[38] Y. Lu, N. Zhang, Q. Zhao, J. Liang, J. Chen, *Nanoscale* **2015**, *7*, 2770.

[39] Y.-T. Weng, T.-Y. Huang, C.-H. Lim, P.-S. Shao, S. Hy, C.-Y. Kuo, J.-H. Cheng, B.-J. Hwang, J.-F. Lee, N.-L. Wu, *Nanoscale* **2015**, *7*, 20075.

[40] C. Zhu, P. Kopold, W. Li, P. A. van Aken, J. Maier, Y. Yu, *J. Mater. Chem. A* **2015**, *3*, 20487.

[41] V. Bodenez, L. Dupont, M. Morcrette, C. Surcin, D. W. Murphy, J. M. Tarascon, *Chem. Mater.* **2006**, *18*, 4278.

[42] R. E. Doe, K. A. Persson, Y. S. Meng, G. Ceder, *Chem. Mater.* **2008**, *20*, 5274.

[43] R. Khatib, A. L. Dalverny, M. Saubanère, M. Gaberscek, M. L. Doublet, *J. Phys. Chem. C* **2013**, *117*, 837.

[44] P. Liu, J. J. Vajo, J. S. Wang, W. Li, J. Liu, *J. Phys. Chem. C* **2012**, *116*, 6467.

[45] H. C. Yu, C. Ling, J. Bhattacharya, J. C. Thomas, K. Thornton, A. Van der Ven, *Energy Environ. Sci.* **2014**, *7*, 1760.

[46] W.-H. Ryu, J. Shin, J.-W. Jung, I.-D. Kim, *J. Mater. Chem. A* **2013**, *1*, 3239.

[47] G. Du, X. Liu, Y. Zong, T. S. A. Hor, A. Yu, Z. Liu, *Nanoscale* **2013**, *5*, 4657.

[48] A. Kocijan, I. Milošev, B. Pihlar, *J. Mater. Sci.: Mater. Med.* **2004**, *15*, 643.

[49] L. E. Klebanoff, D. G. Van Campen, R. J. Pouliot, *Phys. Rev. B* **1994**, *49*, 2047.

[50] L. Dahéron, R. Dedryvère, H. Martinez, M. Ménétrier, C. Denage, C. Delmas, D. Gonbeau, *Chem. Mater.* **2008**, *20*, 583.

[51] S. A. Chambers, R. F. C. Farrow, S. Maat, M. F. Toney, L. Folks, J. G. Catalano, T. P. Trainor, G. E. Brown Jr., *J. Mag. Mag. Mater.* **2002**, *246*, 124.

[52] J.-K. Chang, C.-M. Wu, I. W. Sun, *J. Mater. Chem.* **2010**, *20*, 3729.

[53] P. Hartmann, C. L. Bender, M. Vračar, A. K. Dürr, A. Garsuch, J. Janek, P. Adelhelm, *Nat. Mater.* **2013**, *12*, 228.

[54] Q. Sun, Y. Yang, Z.-W. Fu, *Electrochem. Commun.* **2012**, *16*, 22.

[55] R. M. Cohen, *Mater. Sci. Eng.: R* **1997**, *20*, 167.

[56] S. Tsuzuki, W. Shinoda, H. Saito, M. Mikami, H. Tokuda, M. Watanabe, *J. Phys. Chem. B* **2009**, *113*, 10641.

[57] B. F. Johannesson, *Cement Concrete Res.* **1999**, *29*, 1261.

[58] Y. Jiang, M. Hu, D. Zhang, T. Yuan, W. Sun, B. Xu, M. Yan, *Nano Energy* **2014**, *5*, 60.

[59] K. C. Klavetter, S. Garcia, N. Dahal, J. L. Snider, J. P. de Souza, T. H. Cell, M. A. Cassara, A. Heller, S. M. Humphrey, C. B. Mullins, *J. Mater. Chem. A* **2014**, *2*, 14209.

[60] H. Kim, I. Park, D.-H. Seo, S. Lee, S.-W. Kim, W. J. Kwon, Y.-U. Park, C. S. Kim, S. Jeon, K. Kang, *J. Am. Chem. Soc.* **2012**, *134*, 10369.

[61] Á. Ravel, M. Newville, *J. Synchrotron Radiat.* **2005**, *12*, 537.